A Steering Model of Endothelial Sheet Migration Recapitulates Monolayer Integrity and Directed Collective Migration[▽][†]

Philip Vitorino,*‡ Mark Hammer,‡ Jongmin Kim, and Tobias Meyer*

Chemical and Systems Biology, Bio-X Program, Stanford University, 318 Campus Drive, Stanford, California 94305-5439

Cells in endothelial cell monolayers maintain a tight barrier between blood and tissue, but it is not well understood how endothelial cells move within monolayers, pass each other, migrate when stimulated with growth factor, and also retain monolayer integrity. Here, we develop a quantitative steering model based on functional classes of genes identified previously in a small interfering RNA (siRNA) screen to explain how cells locally coordinate their movement to maintain monolayer integrity and collectively migrate in response to growth factor. In the model, cells autonomously migrate within the monolayer and turn in response to mechanical cues resulting from adhesive, drag, repulsive, and directed steering interactions with neighboring cells. We show that lateral-drag steering explains the local coordination of cell movement and the maintenance of monolayer integrity by allowing closure of small lesions. We further demonstrate that directional steering of cells at monolayer boundaries, combined with adhesive steering of cells behind, can explain growth factor-triggered collective migration into open space. Together, this model provides a mechanistic explanation for the observed genetic modularity and a conceptual framework for how cells can dynamically maintain sheet integrity and undergo collective directed migration.

Endothelial cell monolayers are specialized epithelia that line the luminal surfaces of blood vessels. Functionally, their role is to provide a barrier to retain plasma components in circulation while regulating the exchange of cells and biomolecules between blood and tissues. Dysfunction of this barrier has, for example, been implicated in a number of human diseases, including atherosclerosis (17) and respiratory distress syndrome in the lung (23). Though some epithelial sheets remain fairly static (14), individual endothelial cells can be motile and have been shown to migrate randomly within an intact monolayer *in vitro* (22) and during development of the vasculature *in vivo* (20). This dynamic planar migration maintains the integrity of the monolayer in a process that likely involves dynamic cadherin turnover at cell junctions (15). Furthermore, endothelial cell movements within a monolayer are locally coordinated, with streams of adjacent cells moving in similar directions (20, 22). In addition to this constitutive migration, blood vessels also respond to growth factors, such as fibroblast growth factor (FGF) and vascular endothelial growth factor (VEGF), to induce collective, directed cell movements during wound healing and sprouting angiogenesis.

A recent small interfering RNA (siRNA) screen, by our group, of growth factor-triggered endothelial sheet migration showed that genes that regulate collective migration can be assigned to three specific functional groups, or modules (22). In particular, we identified a group of genes controlling autonomous random migration of cells within monolayers by directing membrane protrusion at the fronts of motile cells; this group includes genes such as those encoding Rac, Cdc42, and Arp2/3, cytoskeletal regulators critical for cell motility (9, 22). The second functional module we identified was responsible for mediating flow-like coordination of cell movement within sheets and was comprised of genes such as those encoding α-catenin and VE-cadherin, known to be involved in cell adhesion (1, 22). The final module of genes was responsible for growth factor-mediated collective migration of the sheet into open space and was comprised of genes encoding the FGF receptor and its downstream modulators (Fig. 1A). In this paper, we hypothesize that the functional groupings derived from the above-mentioned genetic screen can provide a simple framework for a model of collective migration. We present such a model by mapping a particular functional group via its function to a mechanical term in a quantitative model for collective sheet migration.

MATERIALS AND METHODS

Cell culture and transfection. Human umbilical vein endothelial cells (HUVEC) were cultured at 37°C and 5% CO_2 using an EGM Bullet Kit (Lonza). The cells were plated at 10,000 cells per well in a Costar 96-well clear-bottom plate that was coated with 300 μg/ml collagen I (PureCol) for 1 h. For knockdown experiments, cells were transfected with 40 nM siRNA 16 h after being plated with Lipofectin (Invitrogen) according to the manufacturer's protocol. Pools of siRNA were generated from an ~500-bp PCR product and were transcribed, diced, and purified *in vitro* according to the method of Liou et al. (16a). Cell assays were performed 48 to 72 h after siRNA transfection, when protein knockdown is optimal. For cell assays, cells were incubated for at least 4 h in Endothelial SFM (Gibco) that was supplemented with 0.1% bovine serum albumin (BSA) with or without 2 ng/ml basic FGF (bFGF) (Invitrogen), for serum free or growth factor-stimulated experiments.

Sheet migration and live-cell imaging. For sheet migration assays, cells were stained for 20 min with 10 μg/ml wheat germ agglutinin conjugated to Alexa Fluor 594 (Invitrogen) and then scraped. The monolayers were washed three times with phosphate-buffered saline (PBS) and imaged. After 15 h of incubation, the cells were fixed with 4% paraformaldehyde and stained with fluorescein-

* Corresponding author. Mailing address: Chemical and Systems Biology, Bio-X Program, Stanford University, 318 Campus Drive, Stanford, CA 94305-5439. Phone: (650) 725-6926. Fax: (650) 725-2952. E-mail for Philip Vitorino: pvitorino@gmail.com. E-mail for Tobias Meyer: tobias1@stanford.edu.

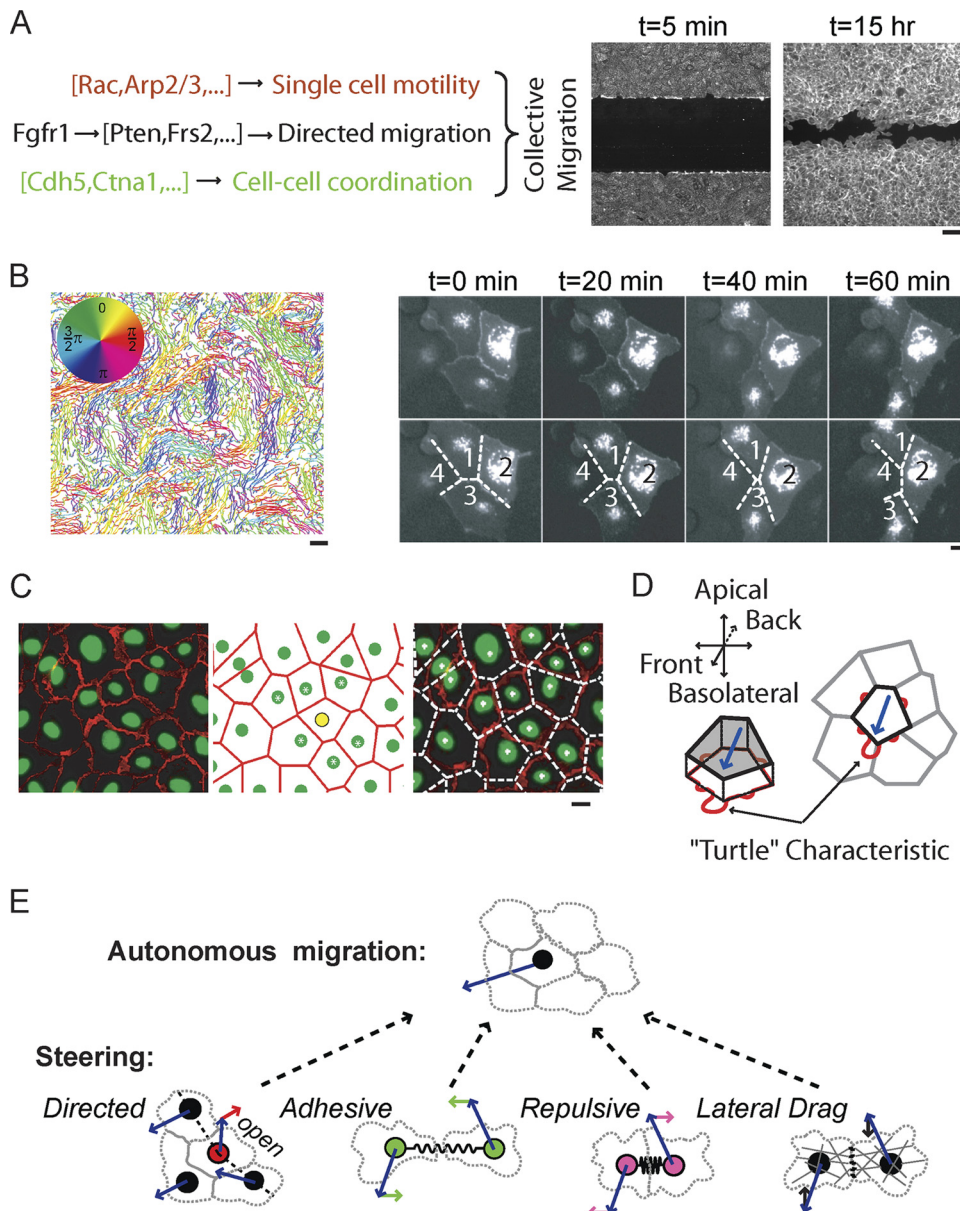‡ P.V. and M.H. contributed equally to this work.

FIG. 1. Experimental and conceptual bases for the endothelial steering model. (A) Classes of genes regulating collective endothelial migration (for further details, see reference 22). (Right) Scratch assay for endothelial sheet migration. Shown are images before and after addition of growth factor displaying growth factor-triggered migration. Bar, 150 μm. (B) (Left) Individual tracks of hundreds of cells in a HUVEC monolayer imaged every 20 min for 15 h. The tracks are colored according to the direction of migration to highlight coordinated movement of neighboring cells. Bar, 150 μm. (Right) Time lapse fluorescence images of HUVEC expressing GFP–VE-cadherin showing vertex-switching events as cells pass each other in a sheet. Bar, 25 μm. (C) (Left) Immunofluorescence image showing cell nuclei stained with Hoescht (green) and adherens junctions stained with anti-VE-cadherin antibody (red). (Middle) Predicted cell boundaries (red lines) derived from Voronoi tessellation of nuclear centroids (green circles). Cell nuclei highlighted with white asterisks represent the neighbors of the yellow cell. (Right) Overlay of measured and predicted cell boundaries. Bar, 25 μm. (D) Schematic representation of the "turtle" characteristic of autonomously migrating cells, where cell motility is generated at the basolateral surface through lamellipodial extensions while cell contacts above remodel to maintain tight barriers. (E) Schematics of the four steering mechanisms that turn autonomously migrating cells. The blue arrows are the current directions of migration. Predicted relative contributions from steering terms are represented by arrows.

phalloidin (Invitrogen). Sheet migration rates were calculated by dividing the change in area by the closure time and edge length to determine edge advancement per hour. For live-cell-tracking experiments, cells were stained with 500 ng/ml Hoescht 33342 (Invitrogen) for 1 h and then washed three times with serum-free medium supplemented with 2 ng/ml FGF. The cells were imaged in an ImageXpress 5000A (Axon Instruments/Molecular Devices) every 20 min

with a 4× objective at 37°C and 5% CO_2 for 6 to 12 h. For tracking of migrating monolayers, a scratch was introduced and watched immediately before imaging.

Cell tracking and coordination analysis. Cell trajectories in the live-cell-imaging experiments were determined using tracking software (7). Java-based analysis algorithms were written for the following analyses: coordination for coordinated flow, directed migration for follower behavior, cell triplet analysis

for drag steering, and cell pair analysis for adhesive steering (see reference 22 for experimental coordination analysis and the supplemental materials for the analysis of coordination between cell pairs and triplets).

Computational modeling of endothelial cell monolayers. We used MATLAB for all cell simulations (for details, see the supplemental materials). For starting conditions, we used randomly distributed cells with random velocities centered on the mean. Steering equation 2 (see below) was then used to incrementally calculate and update the position and velocity of each cell. Before a scratch was introduced to a simulated monolayer, the cells were simulated for several hours to allow the cell distributions to equilibrate.

To calculate the contributions from nearby cells, we determined the position of each neighbor. We used Delaunay triangulation, which joins nearest neighbors using optimal geometric constraints. Cell boundaries were determined using the Voronoi tessellation as implemented in MATLAB and described below. A diagram of relevant vectors is presented in Fig. S1F in the supplemental material. For all modeling experiments, the same steering coefficients were used unless otherwise specified in the figure (directed, 7.5; repulsive, 0.2; adhesive, 0.01; drag, 0.6).

RESULTS

Dynamic cell-cell contact changes and monolayer integrity. We used live-cell imaging of HUVEC to understand how cells migrate and pass each other in monolayers without a loss of sheet integrity. Figure 1B, left, shows that neighboring cells in sheets exhibit partial coordination in their direction of migration, while cells further apart are relatively randomly oriented (22). In this representation, cells migrating in the same direction have tracks with the same color. To monitor cell boundaries during this dynamic process, HUVEC monolayers were transiently transfected with green fluorescent protein (GFP)–VE-cadherin, a major component of adherens junctions. Figure 1B, right, and Movie S1 in the supplemental material illustrate the dynamic nature of cell boundary edges and vertices by showing how cell contacts are formed and lost while an unbroken monolayer is maintained. Note that the exchange of cell-cell contacts (Fig. 1B, right) conserves the total number of contacts and vertices in the monolayer. Since a vertex is the meeting point of three edges, one can make use of the Euler characteristic to derive relationships between cell number, N; edges, E; and vertices, V. Planar geometry tells us that the monolayer sheet has to abide by the following endothelial contact identities:

$$E = 3 \times N - 6 \text{ and } V = 2 \times N - 4 \qquad (1)$$

Equation 1 shows that endothelial cells have on average slightly less than six neighbors, since the average number of contacts per cell, which is $2 \times E/N$, or $6 - 12/N$, reduces to ~6 for a large number of cells. This number represents the average number of neighbors over many cells, though an individual cell had anywhere from 3 to over 10 neighbors and changed over time. Thus, a hallmark of dynamic monolayers is variation in cell contact numbers. This implies that ordered structures, such as the hexagonal cells observed in *Drosophila* wing epithelia (6), by necessity reflect static monolayers.

We obtained a simplified model description of these dynamic cell contact changes based on the observation that adherens junctions were close to the midline between the nuclei of neighboring cells (Fig. 1C). This analysis was based on immunofluorescence comparison of nuclear and VE-cadherin antibody staining. This is reminiscent of a previously observed cadherin zippering of individual epithelial cells that form a first contact (1). As described previously (3), this relationship of nuclei to cell boundaries allowed us to make use of the Voronoi tessellation algorithm to draw midlines between cell centroids and to identify cell neighbors in our model. As cells move within the monolayer, these Voronoi-derived graphs recapitulate the vertex-switching behavior shown in Fig. 1B and preserve the endothelial contact identities (equation 1).

Cell autonomous migration and steering. Our previous siRNA screen identified a group of proteins centered on Rac, Cdc42, and Arp2/3 that regulate single-cell motility within the monolayer. A primary role of this module is predicted to be the regulation of actin polymerization and membrane protrusion at the fronts of cells. Such actin-based membrane protrusions must also contact the extracellular matrix to generate traction forces. Consistent with this hypothesis and a report showing "cryptic" lamellipodia extending underneath neighboring cells in migrating epithelial cells (9), we observed polarized cryptic lamellipods in randomly migrating endothelial cells in intact monolayers (see Fig. S1A in the supplemental material). Thus, we envision a "turtle" model whereby cells in a monolayer exhibit two separate motility regimes: the basolateral motility primarily generates autonomous in-sheet migration via contact with the substrate, and the apical motility maintains sheet integrity by remodeling cell-cell adhesive contacts as the cells move within the sheet (Fig. 1D).

A second key assumption of our model was that mechanical and molecular interactions with neighboring cells induce internal cytoskeletal changes and forces that serve as steering cues that turn these autonomously migrating cells in a graded fashion rather than reorienting them. This was in part supported by observations that most cells in sheets migrate persistently and only gradually change direction over a period of more than an hour (Fig. 1B).

The first such mechanical-steering cue was based on the previous finding in our siRNA classification that growth factor signaling-related genes primarily act on cells at sheet boundaries that have lost part of the cell-cell contact (22). This polarized loss of cell-cell adhesion turns the direction of migration toward the cell-free area generated by the cell removal. Indeed, while the locally coordinated migration in sheets was overall random (Fig. 1B), the presence of open space, combined with growth factor, steered these boundary cells and subsequently enabled directed collective migration toward the cell-free area (Fig. 1A, right). Selective growth factor signaling of boundary cells likely results from an inhibitory role of adherens junctions, as a loss of cadherin expression has been shown to increase the activities of several receptor tyrosine kinases (RTK) (19). This led to the plausible assumption, used below, that steering of boundary cells results from enhanced growth factor signaling that provides a directional cue given by the location where adherens junctions are absent.

The siRNA gene classification also included a group of genes that regulated cell-cell coordination inside a monolayer sheet. When we tested different steering mechanisms that could explain local cell coordination (Fig. 1B), we found that a lateral-drag process directed along a cell's contact surface with another cell recreated this behavior. This steering component was also needed to explain a coordination of movement between three colinear cells (see Fig. S1B in the supplemental material). An additional steering term was needed to explain the observation that cells migrating under low-density condi-

tions stay close to neighboring cells once an initial contact is made, resulting in the formation of cell patches. This requires cell-cell adhesion steering distinct from lateral drag. The directions of adhesive and lateral-drag steering are perpendicular to each other. Adhesion steering was also needed to explain that cells following each other move on average faster than those moving away from each other (see Fig. S1C in the supplemental material). The presence of genes such as those encoding VE-cadherin and alpha-catenin in the cell-cell coordination module (22) suggests that both result from the dynamic regulation of adherens junctions.

Finally, in addition to adhesion and lateral drag, a repulsive steering component was included to explain that HUVEC monolayers have a maximal local cell density. Cell sheets with densities exceeding 1,000 cells/mm^2 prevented additional cells from entering the monolayer (see Fig. S1D in the supplemental material).

Quantitative steering model for endothelial sheet migration. Our sheet migration model was created by combining the autonomous migration process with the four steering interactions detailed above (Fig. 1E). The main assumptions of the model were that individual cells in a sheet move autonomously, dynamically change cell contacts through a vertex-switching mechanism, and are subject to interactions with other cells. We assumed that these mechanical and molecular interactions with other cells are converted into a steering response that alters internal forces and the adhesion dynamics between a cell and the underlying matrix (8), much like the turning behavior observed for cells pulled with microtweezers or exposed to directed fluid flow (16, 21). Of note, we acknowledge the complexity of the biomechanical process of cell migration in sheets. Rather than generating an explicit molecular model describing the intracellular, intercellular, and cell matrix forces involved, our goal was to generate a conceptually simple model with a minimal set of mechanistic terms that reflect classes of genes and that together can explain the main features of the observed collective migration behaviors.

The observed autonomous migration within the sheet was included in the model as a term that slowly enhances or reduces cell speed toward a mean value ($B_{\text{basal\_migration}}$). Mechanistically, this term is derived from the activity of cytoskeletal regulators, such as Rac and Arp2/3, corresponding to the basal migration module identified in the previous siRNA screens (22). Furthermore, the autonomously migrating cells gradually turn in response to the three steering cues that involve direct contact interactions with neighboring cells: adhesion, lateral drag, and repulsion (S_{adhesive}, S_{drag}, and $S_{\text{repulsive}}$). Proteins associated with cell-cell interactions, such as Cdh5 and Ctna1, are responsible for drag and adhesive steering, together comprising another previously identified module (22). It is plausible that the adhesion term corresponds to static cell-cell adhesion and the drag term to the dynamic turnover of cell-cell adhesions. Most of the previously identified genes that alter sheet density (such as the cyclin D gene) likely indirectly affect repulsive interactions as a result of a density change. In the presence of open space, directional steering adds a fourth steering component by selectively orienting cells at the boundary in response to growth factor signals through the activity of downstream signaling proteins, such as Frs2 and Pten (S_{directed}). We assumed that the steering contributions are ad-

ditive, with the sum of all terms affecting both the direction and amplitude of basal migration, giving the following equation for the acceleration (dv/dt) of a particular cell in the sheet:

$$dv_i/dt = \sum_j (S^{ij}_{\text{adhesive}} + S^{ij}_{\text{drag}} + S^{ij}_{\text{repulsive}}) + S^i_{\text{directed}}$$
$$+ B^i_{\text{basal\_migration}} \tag{2}$$

where i and j denote the central cell and its neighbor, respectively.

Steering contributions were approximated using experimental data derived from live-cell tracking experiments in HUVEC. Detailed descriptions of the four steering terms and equations can be found in the supplemental materials and vector nomenclature in Fig. S1E in the supplemental material. In short, initial cell positions and velocities were selected randomly, with cell speed matching the distribution observed within migrating HUVEC monolayers. Based on the positions and velocities of neighbors, individual cell steering terms were then calculated to determine the cell acceleration vector according to equation 2. We assumed that the drag steering term was parallel to the edge between two cells and had amplitude proportional to both the length of the shared edge and the difference in the cell velocity components projected onto this edge. Adhesive steering was parallel to the connecting centroid vector with amplitude proportional to the length of the edge and the centroid distance (up to a maximal reach). Analogously, repulsive steering had the same direction but decreased linearly with centroid distance. Finally, directional steering toward the open space was selectively engaged when more than half of the cell contacts to neighbors were lost. Whenever possible, parameters such as maximal reach and repulsive distances were determined experimentally by monitoring HUVEC migration at various densities. The relative strength of each steering term was selected based on its ability to recapitulate simple monolayer behaviors, such as cohesion, coordination, and directed movement, and was kept constant for all simulations unless otherwise noted.

Model predictions of collective cell movement. Our first goal was to test whether these simplified assumptions are sufficient to actually show movement of cells within the sheet without causing lesions and to predict different observed sheet migration behaviors. Notably, in the absence of directed motility, the model recapitulated dynamic cell movements within the monolayer, formation and destruction of cell contacts, and maintenance of sheet integrity. In addition, the model monolayer displayed no migration into open space, resembling *in vitro* behavior in the absence of growth factors (Fig. 2A, left). In contrast, when cells along the sheet boundary were allowed to undergo directional steering (reflecting the presence of growth factor), the simulated monolayer migrated collectively, eventually repopulating the cell-free area, again without losing sheet integrity (Fig. 2A, right; see Movie S2 in the supplemental material).

We investigated the different steering contributions by displaying the dominant steering cue as a colored vector arrow. In the absence of directional steering, adhesion is the dominant steering interaction at the sheet boundary, and as expected, it prevented stochastic extensions into cell-free space (Fig. 2A, bottom left, green arrows). In the presence of directional steering, a fraction of the cells at the sheet boundary triggered
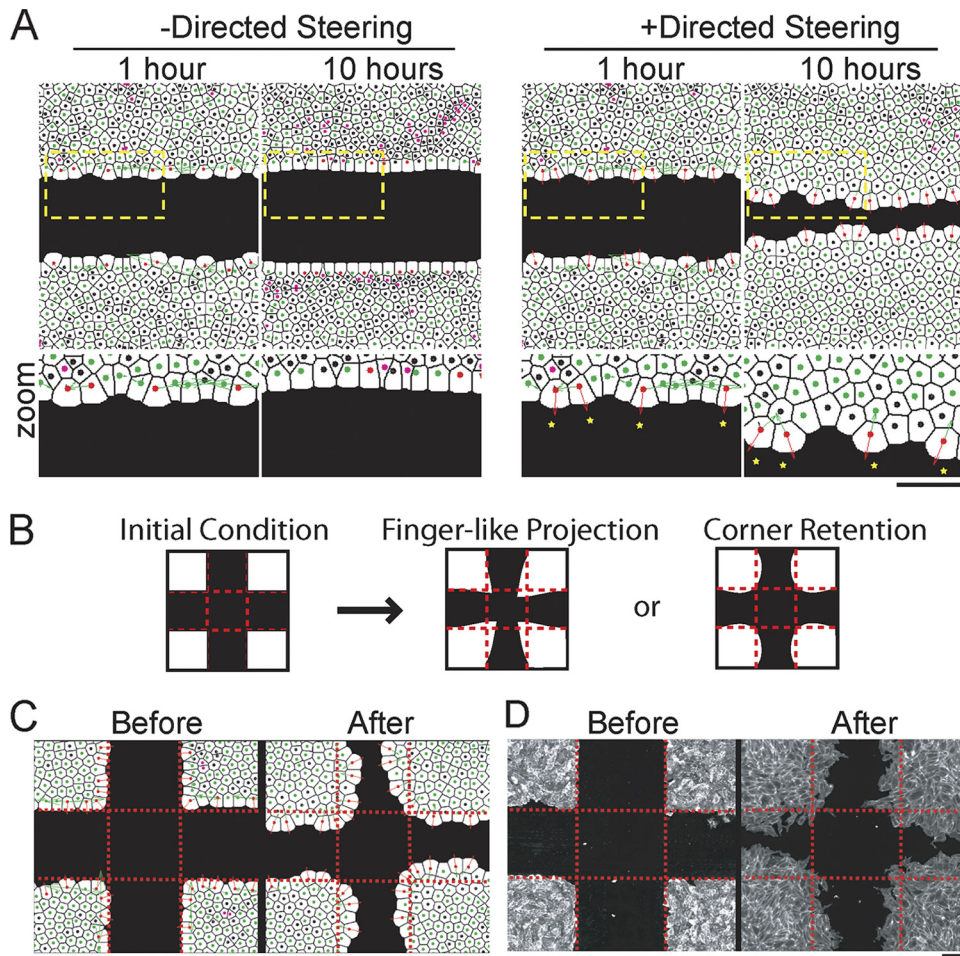
FIG. 2. Steering model predicting collective endothelial migration behaviors. (A) Computational cell monolayers respond to a large open space over 10 simulated hours in the absence (left) and presence (right) of growth factor. Enlargements of the regions outlined by yellow dashes are shown below. The colors of the nuclei indicate the dominant steering type: green, adhesive; red, directed; magenta, repulsive; and black, lateral drag. The arrows illustrate the direction and magnitude of steering terms. (B) Schematic representation of two possible migration outcomes for monolayers starting with triangular projections: finger extension versus corner retention. (C) Images of simulated monolayers responding to a cell-free area with pioneer cells at artificially generated triangular corner positions. The snapshots represent cells immediately after the introduction of cell-free space and after a simulated 12-h period, showing corner retention. (D) HUVEC subjected to a cross scratch that generated triangular projections before and after a 12-h incubation period, showing corner retention. The cells were assayed as in Fig. 1A. Bars, 150 μm.

directional steering (Fig. 2A, bottom right, yellow stars), counteracting the adhesive steering and thereby promoting collective migration (Fig. 2A, bottom right, green arrows). Together, this showed that modeling of mechanical parameters based on siRNA-based classification and mapping these functional classes to a simple mechanical model were sufficient to explain key sheet migration behaviors.

Migration measurements showed that cells at the sheet boundary often generate extensions into the cell-free space that resemble triangular projections (Fig. 1A, right). We tested whether our model could predict sheet movement when cells were positioned artificially at the tip of a protruding triangle. This morphological patterning was achieved by scraping two perpendicular lines into the monolayer so that the resulting monolayer was organized into 90° angles (Fig. 2B, left). Our intuition would have predicted that corner cells would be primed and further increase the length of the preformed pro-

jection (Fig. 2B, middle). However, the model predicted that conflicting directional cues from corner cells and linear surfaces would steer the sides of the monolayer into the open space and thereby limit forward movement of the corner cells (Fig. 2B, right, and C). Indeed, HUVEC exhibit a migration pattern consistent with the modeling data, suggesting that adhesive steering can ultimately restrain cell movements at corner positions, a mechanism that may prevent cells from escaping from the monolayer and foster more uniform directed migration of endothelial cell monolayers (Fig. 2D). This demonstrated that the model can be used to evaluate migration behaviors for alternative monolayer geometries.

Adhesive steering drives follower behavior and promotes sheet cohesion. We then applied the model to gain insights into which steering processes may primarily contribute to follower behavior of cells inside the monolayer (for schematics, see Fig. S1G in the supplemental material). Directional movement was
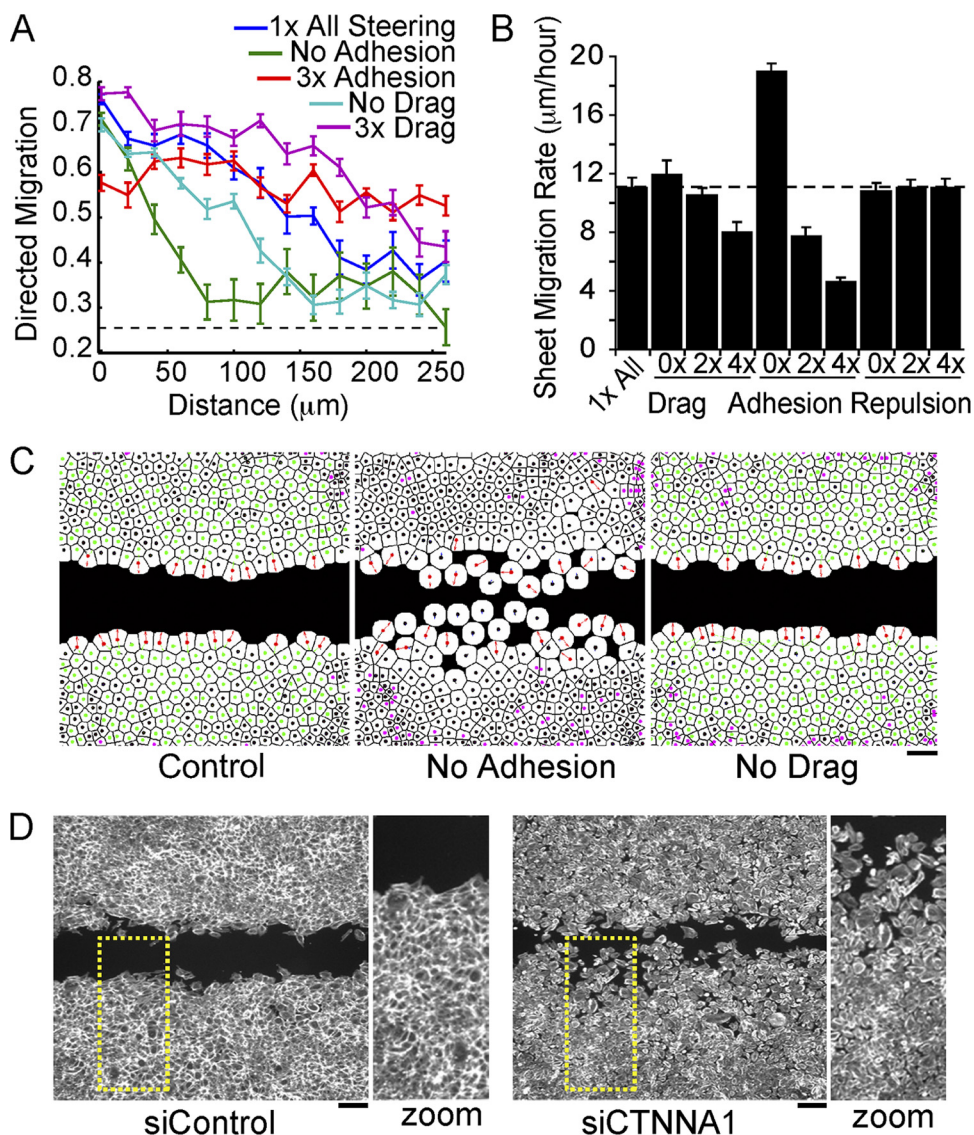
FIG. 3. Adhesive steering mediates follower behavior during directed sheet migration. (A) Directed migration as a function of distance from the cell-free area. Directed migration is defined as the fraction of time a cell spends moving toward the cell-free area (see the text). (B) Sheet migration rates for monolayers simulated with indicated relative changes to steering terms. The sheet migration rate was calculated as the average progression of the sheet boundary per hour. (C) Images from migrating monolayers run for 10 simulated hours for control (left), no adhesion (middle), and no drag term (right), suggesting that adhesion is important for sheet cohesion. (D) HUVEC monolayer transfected with control siRNA (siControl) or siRNA targeting alpha-catenin (siCTNNA1), a regulator of cell-cell junctions, fixed 15 h after the introduction of cell-free space and stained with fluorescein-phalloidin, showing loss of cohesion. Zoom, enlargements of the areas outlined by yellow dashes. All measurements represent the average of three replicates with error bars indicating standard errors. Bars, 150 μm.

defined as the fraction of cells moving toward the cell-free space within a 90° window. Similar to experimental data (22), the model predicted that cells along the boundary were the most directed, and directed motility propagated up to 200 μm into the cell monolayer (Fig. 3A, blue line). Randomly moving cells would be expected to move toward the open space 25% of the time (dashed line). When adhesion-mediated steering was removed from the model, cells at the boundary remained directed, but follower behavior did not propagate beyond the boundary cells (Fig. 3A; green line). When adhesive steering was increased, cells over 250 μm from the sheet boundary exhibited directional movements (Fig. 3A, red line), al-

though the entire sheet migrated more slowly (Fig. 3B). Conversely, a decrease in adhesion strength led to an increase in the speed of sheet migration. Lateral drag and repulsive steering had much smaller effects on follower behavior (Fig. 3A and B).

We further differentiated the roles of adhesion and lateral drag by removing each steering term and visualizing changes in sheet cohesion. While removing adhesion caused many cells to break away from the sheet, removing lateral drag had less of an effect (Fig. 3C). Though there is currently no experimental way to alter adhesive steering without affecting lateral drag, we used siRNA to knock down alpha-catenin, a gene necessary for
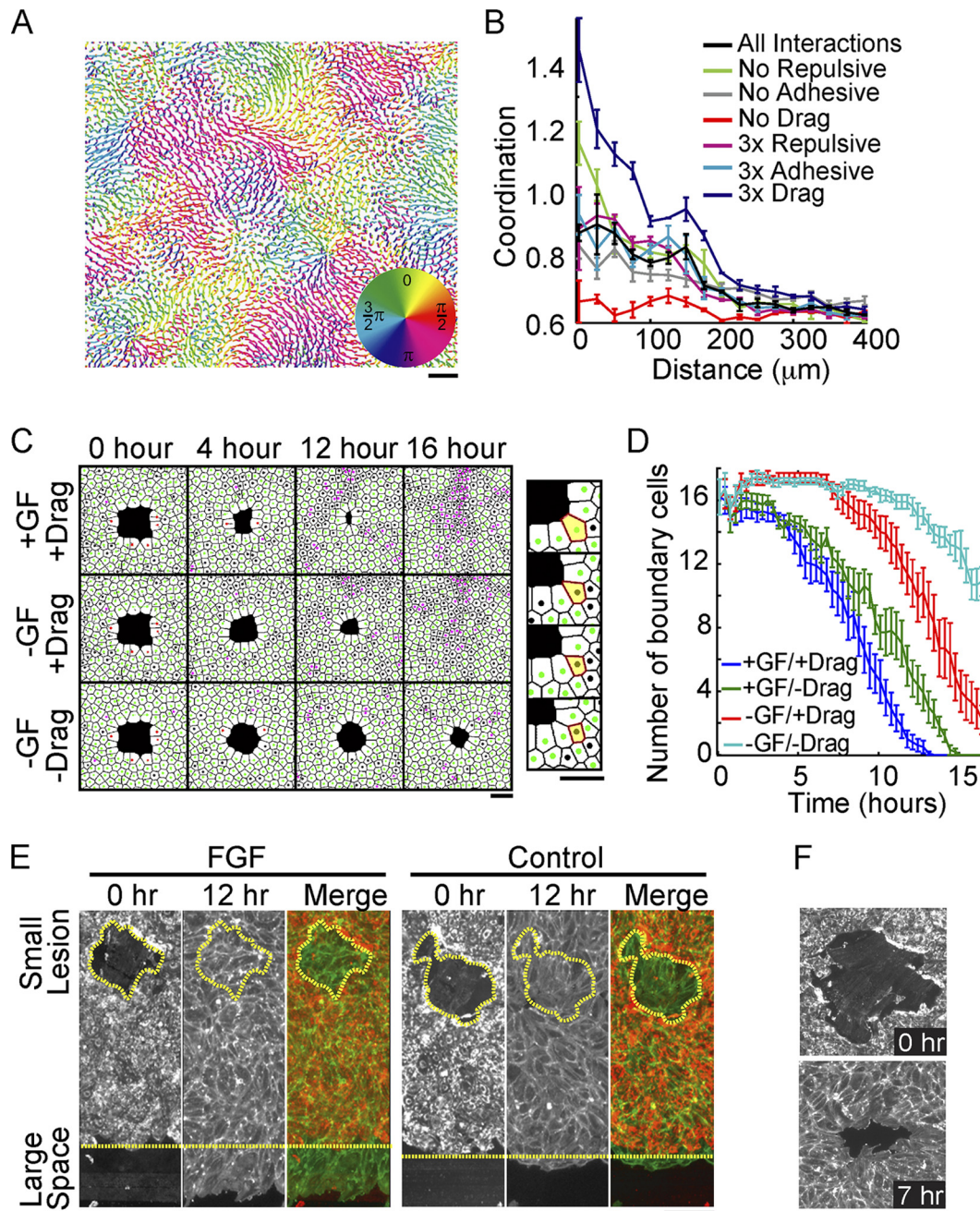
FIG. 4. Drag mediates coordinated migration and small-lesion closure even in the absence of directed motility. (A) Cell tracks from a computational model run for 16 simulated hours colored according to the direction of migration. (B) Quantification of coordinated migration in simulated tracks with indicated relative steering changes (for details, see the text). (C) Images of cell monolayers derived from the computational model representing 0, 4, 12, and 16 simulated hours after the introduction of a small lesion. Steering terms were included (+) or eliminated (−) as indicated. (Right) Zoomed image of a simulated monolayer with an excluded boundary cell highlighted in yellow. (D) Number of boundary cells surrounding a small lesion plotted as a function of time for different steering conditions, suggesting that drag helps to reduce the number of cells bordering small lesions. All measurements represent the averages of three replicates, with error bars indicating standard errors. (E) Differential migration into small and large open spaces. Cells were assayed as in Fig. 1D in the presence (left) and absence (right) of FGF. Merge, merged image of the monolayer before (red) and after (green) a 12-hour migration period, showing that small lesions can close in the absence of directed migration. The perimeter of the small wound and edge of the sheet boundary are marked with yellow dashed lines. (F) Phalloidin staining for polymerized actin in endothelial cells surrounding a small lesion showing no apparent actomyosin ring, supporting a migration- over a constriction-based closure mechanism. Bars, 150 μm.

the establishment of cell-cell contacts, and found fragmented monolayers where cells moved into the cell-free space individually (Fig. 3D). This suggested that adhesive steering plays a key role in collective migration. Together with the results men-

tioned above, these calculations show that long-range signaling is not needed to generate collective migration. Instead, the observed collective directed migration behavior can simply be explained by directed migration of boundary cells combined

with local cell adhesion steering of autonomously migrating cells inside the monolayer.

Lateral drag and constitutive migration facilitate the closure of small lesions. Lateral-drag steering had to be included in the model to generate the observed locally coordinated migration in the presence or absence of growth factor (Fig. 1B). Plots of the analogous coordinated flow within model monolayers are shown in Fig. 4A. To quantify coordination in these simulations, we determined the angular difference between velocity vectors for every cell pair as a function of their distance apart. For clarity, we plotted the inverse of this difference so that a higher value on the *y* axis corresponded to increased coordination ($2/\pi = 0.64$ is random). Consistent with experimental observations (22), coordination between cells was high over short distances and random over distances greater than 200 μm (Fig. 4B, "control" black line). Consistent with a primary role of lateral drag, only increasing or decreasing lateral drag resulted in a strong increase and decrease in cell-cell coordination, respectively (Fig. 4B, dark-blue versus red lines).

Though drag-mediated steering is sufficient to explain coordinated flow, the physiological relevance of this behavior remained unclear. We hypothesized that locally coordinated flow may accelerate the closure of small lesions, which form frequently in the endothelial lining of the vasculature (13). Consistent with experimental data, in the absence of directed steering, model sheets failed to migrate into large open spaces (Fig. 2A), while in the presence of directed steering, large or small lesions readily closed (Fig. 4C; see Movie S3 in the supplemental material). Nevertheless, a surprising result was that small lesions still effectively closed in the absence of directed steering in a process that required lateral-drag steering (Fig. 4C).

This role of drag in small-lesion closure might be linked to the expulsion of boundary cells (Fig. 4C, right, yellow cell), which lack a cell contact when they border the lesion. This lack of a contact leaves drag unbalanced, leading to a movement that is more often tangential to the lesion. As a result of this bias, cells more frequently leave the lesion boundary, allowing the remaining cells to contract further (Fig. 4D). Notably, the boundary of a large open space lacks the necessary curvature between cells, so single-cell exclusion events do not encourage closure, which explains why lateral drag does not close large wounds. Given this prediction, we tested whether real endothelial sheets could close small lesions in the absence of growth factor. For comparison, we introduced a large horizontal cell-free space alongside the smaller lesion. In the presence of FGF, the sheet migrated into the large wound and completely filled the small lesion (Fig. 4E, left). Strikingly, in the absence of FGF, there was no sheet migration into the large open space, but the small lesion still closed after 12 h (Fig. 4E, right). This confirms that monolayers can close small open spaces even in the absence of growth factor signals. Of note, small-lesion closure by a process involving a contracting perimarginal actomyosin purse string has been observed in epithelial sheets (4, 10). In HUVEC, however, cells surrounding a small lesion do not form a visible actin ring structure, as visualized with phalloidin staining (Fig. 4F), suggesting that purse string closure is less important in these endothelial monolayers.

Repulsion and adhesion determine the elasticity of endothelial monolayers. At the density used for the model calculations discussed above, repulsive steering had no significant impact on migration rates (Fig. 3B). Also, when growth factor stimuli are absent, cells at an optimal density do not migrate into the open space (21). This suggests that previous models that were based on an expansion of compressed monolayers (2) cannot fully explain the experimental behavior of endothelial sheets. Nevertheless, HUVEC can be plated from 250 up to 1,000 cells/mm^2 and still form an intact monolayer, suggesting that monolayers exhibit remarkable elasticity, likely supported by adhesive and repulsive steering. Indeed, when cells are plated at densities higher than the contact-arrested levels of ~700 cells/mm^2, growth factor-dependent and -independent sheet migrations were significantly increased (see Fig. S2A and B in the supplemental material). This plausibly explains some of the reported repulsive behavior associated with directed sheet migration (2) and argues that elasticity and compressibility are important properties of endothelial sheets. Furthermore, repulsion also enforced uniform cell distribution, since model monolayers have more realistic uniformly distributed cells only in the presence of repulsive steering (see Fig. S2C and D in the supplemental material). Thus, a role for repulsive steering is to expand cells in a compressed area, both locally in high-density patches and globally during sheet extension if sheets have an increased cell density.

DISCUSSION

We have developed a steering model for endothelial sheet migration based on autonomously migrating cells that turn their direction of migration in response to four interactions: adhesive, repulsive, lateral drag, and directed steering. These four steering terms were necessary and sufficient to reproduce growth-factor triggered collective migration and coordinated motility inside cell monolayers, explaining how sheets can maintain their barrier function, create uniform cell distribution, collectively migrate, and close small lesions. This builds a conceptual framework for the cell dynamics that underlie endothelial function and suggests further avenues of investigation regarding the molecular mechanisms of migration and steering.

Methodologically, this showed that classes of genes derived from siRNA screens can be mapped to mechanical terms that quantitatively describe a complex cellular process. It also supports a more general assumption in biology that cells use genetically modular control processes to generate complex systems behaviors.

Insights into growth factor-triggered directional migration of boundary cells and follower behavior. Endothelial cell monolayers move collectively in response to growth factors, which is required *in vivo* to repair existing vasculature and to generate new blood vessels. Our model simulations show that directed motility in boundary cells is sufficient to generate movement of an entire interconnected monolayer. Directional information is passed from the cells at the boundary that are directed by growth factor signaling (pioneer cells) to follower cells primarily through adhesive steering, with a weak contribution from drag-mediated steering (Fig. 5, top). As pioneer cells set the direction of migration, boundary cells begin to pull on trailing cells, biasing their movements in the forward direction. These cells in turn steer the cells behind them, allowing local cell interactions to mediate collective sheet migration.

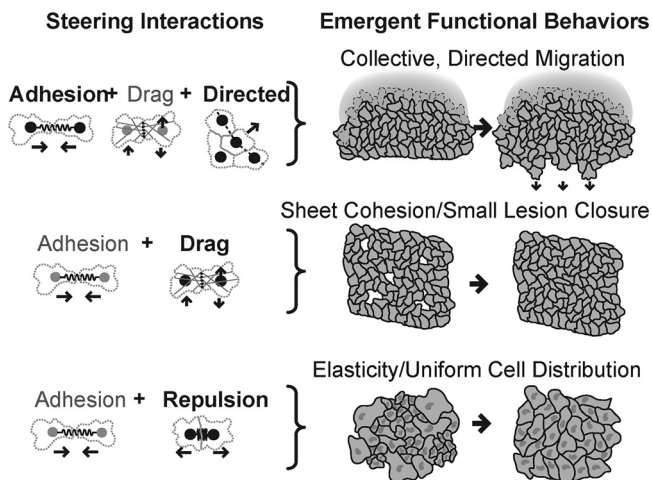A similar process may apply to vessel sprouting during angio-

FIG. 5. Four steering mechanisms are necessary and sufficient to generate sheet cohesion; elasticity; and collective, directed migration. Shown is a schematic representation of emerging monolayer functions. The dominant steering terms are indicated in boldface.

genesis. In response to VEGF signaling, a subset of endothelial cells exhibited high filopodial activity (11), analogous to FGF-induced pioneers in HUVEC sheets. As these "tip cells" migrate, adjoining "stalk cells" follow, providing the foundation for a future blood vessel (12). These stalk cells resemble boundary cells in HUVEC that are not responsive to FGF but are still directed into cell-free space by adjacent pioneers. Our study suggests that tip-to-stalk directional information can be passed through direct biomechanical adhesive steering and, to a lesser extent, lateral drag and may not require diffusive directional signals.

Insights into the maintenance of the endothelial barrier function. Endothelial barriers play a key role in regulating the flow of material between the circulating blood and tissues, and this function requires sheet integrity. Our modeling and experimental data revealed a novel mechanism for closing small lesions through the activity of lateral-drag-based steering (Fig. 5, middle). Though lateral drag cannot close a large open space, small lesions create a unique geometrical constraint that requires the expulsion of cells from the lesion boundary, and this movement is facilitated by lateral-drag steering. Unlike directed sheet migration, drag-mediated closure does not rely on growth factor signaling, allowing it to function under homeostatic conditions to maintain sheet integrity. When large-scale movements are required during wound healing or angiogenesis, however, cells induce growth factor-mediated directed migration in order to move effectively *in vivo* (5, 18, 24).

Finally, our study showed that continuous random migration within a sheet leads to monolayer elasticity, where adhesive and repulsive steering distribute cells uniformly over a large window of cell densities (Fig. 5, bottom). This elasticity may minimize the likelihood of random tears due to local stress and may confer flexibility to accommodate local pressure changes during rapid vessel deformations.

Conclusions. While individual cells within monolayers must coordinate their activities to preserve appropriate tissue structure, the mechanisms by which cells in a monolayer communicate with one another has been largely elusive. Here, we have shown that a set of local steering terms that govern the directional

choices of otherwise autonomously migrating cells is sufficient to predict many observed random, coordinated, and directed migration behaviors in cultured endothelial cell monolayers. Thus, we show that a modular conceptual understanding of a biological process, based on underlying genetic data, can predict real cell behavior, elucidate the purpose of important low-level functions, and suggest avenues for future experimentation.

REFERENCES

1. **Adams, C. L., W. J. Nelson, and S. J. Smith.** 1996. Quantitative analysis of cadherin-catenin-actin reorganization during development of cell-cell adhesion. J. Cell Biol. **135:**1899–1911.
2. **Bindschadler, M., and J. L. McGrath.** 2007. Sheet migration by wounded monolayers as an emergent property of single-cell dynamics. J. Cell Sci. **120:**876–884.
3. **Bock, M., A. K. Tyagi, J. U. Kreft, and W. Alt.** 2010. Generalized Voronoi tessellation as a model of two-dimensional cell tissue dynamics. Bull. Math. Biol. **72:**1696–1731.
4. **Brock, J., K. Midwinter, J. Lewis, and P. Martin.** 1996. Healing of incisional wounds in the embryonic chick wing bud: characterization of the actin purse-string and demonstration of a requirement for Rho activation. J. Cell Biol. **135:**1097–1107.
5. **Carmeliet, P.** 2003. Angiogenesis in health and disease. Nat. Med. **9:**653–660.
6. **Classen, A. K., K. I. Anderson, E. Marois, and S. Eaton.** 2005. Hexagonal packing of Drosophila wing epithelial cells by the planar cell polarity pathway. Dev. Cell **9:**805–817.
7. **Crocker, J. C., and D. G. Grier.** 1996. When like charges attract: the effects of geometrical confinement on long-range colloidal interactions. Phys. Rev. Lett. **77:**1897–1900.
8. **du Roure, O., A. Saez, A. Buguin, R. H. Austin, P. Chavrier, P. Silberzan, and B. Ladoux.** 2005. Force mapping in epithelial cell migration. Proc. Natl. Acad. Sci. U. S. A. **102:**2390–2395.
9. **Farooqui, R., and G. Fenteany.** 2005. Multiple rows of cells behind an epithelial wound edge extend cryptic lamellipodia to collectively drive cell-sheet movement. J. Cell Sci. **118:**51–63.
10. **Fenteany, G., P. A. Janmey, and T. P. Stossel.** 2000. Signaling pathways and cell mechanics involved in wound closure by epithelial cell sheets. Curr. Biol. **10:**831–838.
11. **Gerhardt, H., and C. Betsholtz.** 2005. How do endothelial cells orientate? EXS **94:**3–15.
12. **Gerhardt, H., M. Golding, M. Fruttiger, C. Ruhrberg, A. Lundkvist, A. Abramsson, M. Jeltsch, C. Mitchell, K. Alitalo, D. Shima, and C. Betsholtz.** 2003. VEGF guides angiogenic sprouting utilizing endothelial tip cell filopodia. J. Cell Biol. **161:**1163–1177.
13. **Greenhill, N. S., and W. E. Stehbens.** 1985. Haemodynamically-induced intimal tears in experimental U-shaped arterial loops as seen by scanning electron microscopy. Br. J. Exp. Pathol. **66:**577–584.
14. **Hegerfeldt, Y., M. Tusch, E. B. Brocker, and P. Friedl.** 2002. Collective cell movement in primary melanoma explants: plasticity of cell-cell interaction, beta1-integrin function, and migration strategies. Cancer Res. **62:**2125–2130.
15. **Kametani, Y., and M. Takeichi.** 2007. Basal-to-apical cadherin flow at cell junctions. Nat. Cell Biol. **9:**92–98.
16. **Kolega, J.** 1986. Effects of mechanical tension on protrusive activity and microfilament and intermediate filament organization in an epidermal epithelium moving in culture. J. Cell Biol. **102:**1400–1411.
16a.**Liou, J., M. L. Kim, W. D. Heo, J. T. Jones, J. W. Myers, J. E. Ferrell, Jr., and T. Meyer.** 2005. STIM is a Ca²⁺ sensor essential for Ca²⁺-store-depletion-triggered Ca²⁺ influx. Curr. Biol. **15:**1235–1241.
17. **Nakashima, Y., T. N. Wight, and K. Sueishi.** 2008. Early atherosclerosis in humans: role of diffuse intimal thickening and extracellular matrix proteoglycans. Cardiovasc. Res. **79:**14–23.
18. **Ortega, S., M. Ittmann, S. H. Tsang, M. Ehrlich, and C. Basilico.** 1998. Neuronal defects and delayed wound healing in mice lacking fibroblast growth factor 2. Proc. Natl. Acad. Sci. U. S. A. **95:**5672–5677.
19. **Qian, X., T. Karpova, A. M. Sheppard, J. McNally, and D. R. Lowy.** 2004. E-cadherin-mediated adhesion inhibits ligand-dependent activation of diverse receptor tyrosine kinases. EMBO J. **23:**1739–1748.
20. **Rupp, P. A., A. Czirok, and C. D. Little.** 2004. alphavbeta3 integrin-dependent endothelial cell dynamics in vivo. Development **131:**2887–2897.
21. **Simmers, M. B., A. W. Pryor, and B. R. Blackman.** 2007. Arterial shear stress regulates endothelial cell-directed migration, polarity, and morphology in confluent monolayers. Am. J. Physiol. Heart Circ. Physiol. **293:**H1937–H1946.
22. **Vitorino, P., and T. Meyer.** 2008. Modular control of endothelial sheet migration. Genes Dev. **22:**3268–3281.
23. **Weis, S. M.** 2008. Vascular permeability in cardiovascular disease and cancer. Curr. Opin. Hematol. **15:**243–249.
24. **Werner, S., K. G. Peters, M. T. Longaker, F. Fuller-Pace, M. J. Banda, and L. T. Williams.** 1992. Large induction of keratinocyte growth factor expression in the dermis during wound healing. Proc. Natl. Acad. Sci. U. S. A. **89:**6896–6900.